Royal Aeronautical Society 2018 Applied Aerodynamics Conference
The Future of Aerodynamics–Research, Development, Simulation and Applications
Bristol, UK, 24-26 July 2018

Development and application of WASPE for conceptual design of HEDiP aircraft

R. V. Ganesh
rvg@vt.edu
P. Raj
S. Choi
Kevin T. Crofton Department of Aerospace and Ocean Engineering
Virginia Polytechnic Institute and State University
Blacksburg, Virginia, USA

M. Emeneth
PACE America Inc.
USA

ABSTRACT

In recent years, there has been an increasing emphasis on sustainability in civil aviation. This has motivated new aircraft designs with increased fuel efficiency and reduced emissions. A Hybrid Electric Distributed Propulsion (HEDiP) system offers considerable promise to reduce fuel consumption and emissions. However, the current conceptual design methods are not fully mature for developing optimal HEDiP configurations. Fast and accurate estimation of wing aerodynamic characteristics in the presence of multiple propellers is one of the key needs. This need is fulfilled by the development of WASPE (Wing Aerodynamic Simulation with Propeller Effects), a modified vortex lattice method (VLM). WASPE is coupled with the Pacelab Aircraft Preliminary Design (APD) multidisciplinary design and optimization framework which is then employed to perform conceptual design of a regional transport aircraft using a HEDiP system. The resulting capability offers designers new opportunities of exploring novel designs of more sustainable aircraft.

1.0 INTRODUCTION

The recent years have seen a growing movement to steer the world towards sustainability. For civil aviation, this is reflected in the goals of key organizations, such as NASA [1] and ACARE, in the form of significantly improved fuel efficiency along with reduced harmful emissions and direct heat release in the atmosphere as illustrated in Figure 1. These goals are also supported by the airline industry owing to the positive impact of advanced technologies on the operational cost and the environment.

NASA Targeted Improvements in Subsonic Transport System-level Metrics

TECHNOLOGY BENEFITS	TECHNOLOGY GENERATIONS (Technology Readiness Level = 5-6)		
	Near-term 2015-2025	Mid-term 2025-2035	Far-term Beyond 2035
Noise (cumulative below Stage 4)	22 - 32 dB	32 - 42 dB	42 - 52 dB
LTO NO_x Emissions (below CAEP 6)	70 - 75%	80%	>80%
Cruise NO_x Emissions (relative to 2005 best in class)	65 - 70%	80%	>80%
Aircraft Fuel/Energy Consumption (relative to 2005 best in class)	40 - 50%	50 - 60%	60 - 80%

Figure 1. NASA Subsonic Transport Technology Goals. From NASA [1]

Achieving such ambitious goals necessitates the advent of novel technologies and systems along with radical aircraft concepts driven by efficiency maximization as well as utilization of energy sources other than fuel. NASA's X-57 Maxwell [2], shown in Figure 2, is one such unconventional design that leverages

alternate fuel sources by using a distributed electric propulsion (DEP) system. Borer et al. [3] and Stoll et al. [4] elucidate the benefits of utilizing distributed propulsion. The presence of multiple propellers increases the dynamic pressure over the wing and thereby providing high lift during takeoff. Shutting down for cruise, this allows for a lifting surface design optimally tuned for highly efficient cruise performance.

Figure 2. DEP demonstrated in X-57 Maxwell aircraft. From NASA [2].

Although the concept of distributed propulsion is in existence since the 1920s, application of this technology was restricted by the complexities in distributing traditional propulsors along with penalties in terms of weight, efficiency and cost. These penalties can be overcome by using electric motors with their scale invariant performance, independence of power generation to altitude, and faster response time. Also, electric motors are lighter and more compact than traditional powerplants for the same performance. Therefore environmental benefits in the form of reduced operating noise, lower harmful gas emission and reduced fossil fuel consumption can be realized.

Significantly increased efficiencies of the electric aircraft propulsion systems are highlighted in Figure 3 from the work of Hepperle [5]. Utilization of such battery stored energy extends to the user nearly twice the energy conversion efficiency while at the same time curtailing the nefarious impact of traditional fuel powered air vehicle operations on the environment.

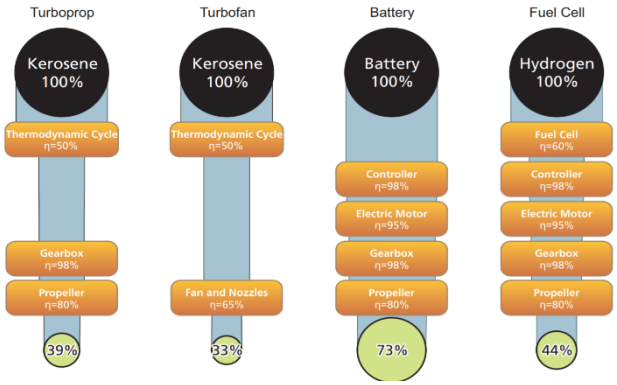

Figure 3. Comparison of propulsive system efficiencies. From Hepperle [5].

Moore and Fredericks [6] discuss innovations, such as DEP, that could systematically utilize projected improvements in electrical storage technologies. Without such innovations, it would be very hard to develop electrical aircraft that could compete with fossil fuel aircraft in any near future. They also clearly articulate the potential of dramatic reductions in energy costs of their LEAPTech concept due to its innovative DEP system in making a very convincing case for continuing to pursue electrical aircraft designs for not just general aviation, but also for commercial transport aircraft. Gohardani [7] also indicates, notwithstanding the power density limitations, that an effective application of DEP could be revolutionary.

1.1 Challenges for All-Electric Aircraft

A substantial challenge for developing all-electric aircraft is the heavy weight penalty associated with energy storage. The Jet A fuels have an energy density of about 11.5 kWh/kg whereas the Lithium-Ion batteries, the best commercially available battery technology for energy storage today, have 0.265 kWh/kg. Although several advancements in battery technologies have shown promising results in laboratory settings, widespread commercial application of such breakthroughs have not yet materialized. The limitations and prospects of electrification are currently limited to ultralights and maybe general aviation aircraft. Nevertheless, several technology demonstrators such as the Pipistrel Alpha Electro and JAXA Feather strongly suggest that exclusive electrical energy utilization cannot be precluded from contemporary aviation.

A recent study by Patterson [8] shows that an all-electric general aviation aircraft using 2050 battery technology would result in half the range of the Cirrus SR22, a conventional hydrocarbon based aircraft,

for comparable gross weight of approx. 3,600 lbs. At least twice the contemporary battery specific energy, i.e., about 0.5 kWh/kg is required for practical usage. An order of magnitude increase in specific energy to about 1.2 kWh/kg is needed for a commercially viable aircraft. This would push feasible application of electric propulsion to well beyond 2050 timeframes.

In the near term, a Hybrid Electric Distributed Propulsion (HEDiP) system offers a promising alternative to the all-electric system. It leverages the benefits of DEP when coupled with a hybrid electric system. Such a system could significantly reduce emissions and fuel burn along with reduced direct atmospheric heat release—the key tenets of minimizing the environmental impact. It would also reduce total energy consumption and total energy costs.

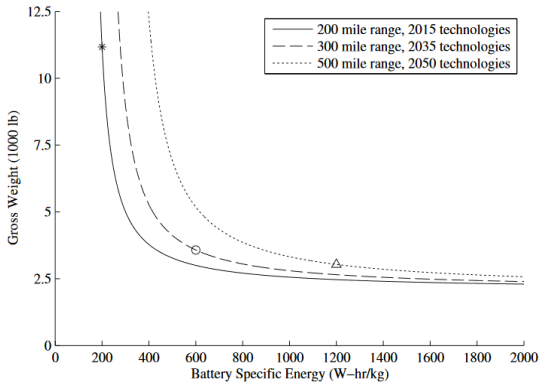

Figure 4. Impact of battery specific energy on electric aircraft gross weight. From Patterson [8].

1.2 Hybrid Electric Propulsion Systems

Several Hybrid-Electric architectures can be utilized for HEDiP. For a thorough investigation of such architectures, the reader is referred to Del Rosario [9], Cinar et al. [10] and Strack et al. [11]. Figure 5 shows four typical architectures, i.e., series, parallel, turboelectric, and parallel power split architectures. The efficiencies of these architectures can be estimated using simple component estimates, assuming equal power contribution by both energy sources, fuel and battery, at sea level [12].

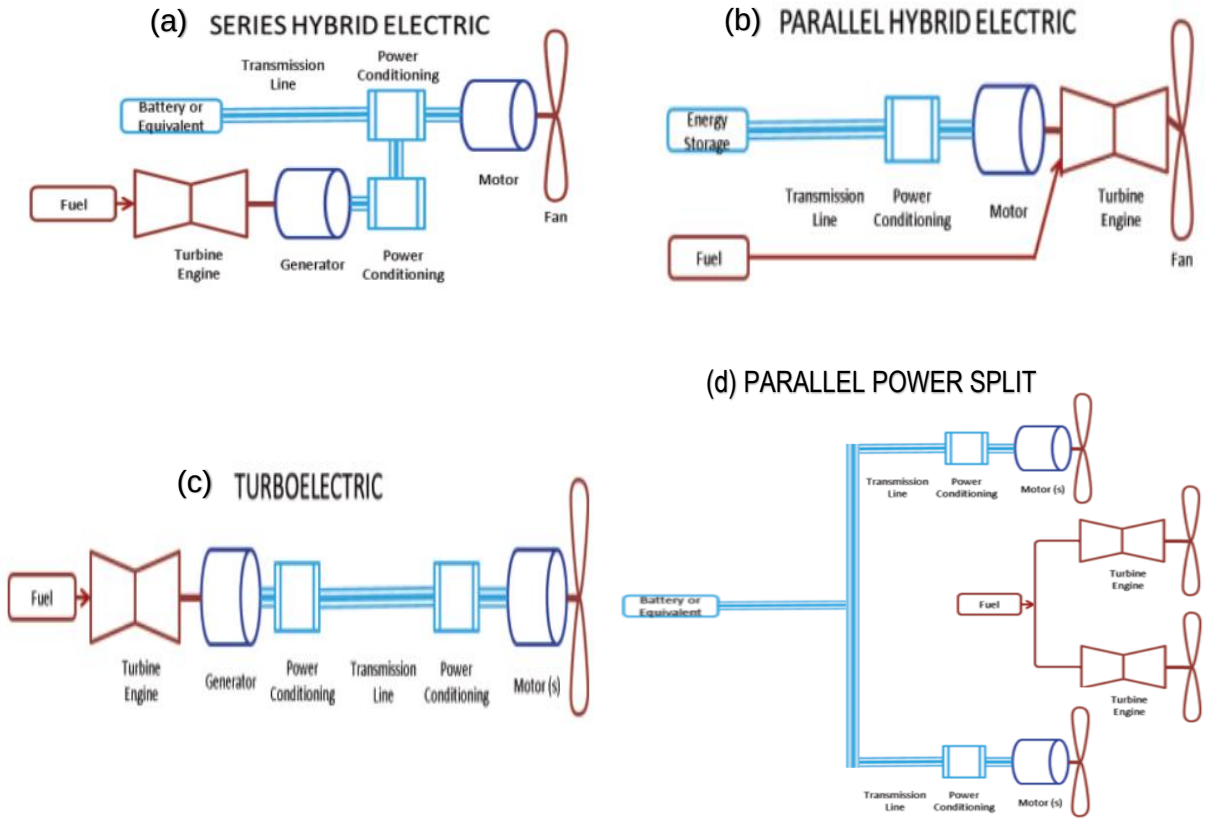

Figure 5. Typical hybrid electric architectures for aircraft. (a) series. (b) parallel. (c) turboelectric. (d) parallel power split. Adapted from Del Rosario [9].

The parallel architecture has an estimated efficiency of 51% while the series architecture has 47%. Notice that the range of efficiencies falls between those of fully electric (~73%) and turboprop (~39%) propulsive systems. The turboelectric architecture has an efficiency of 31% which is less than that of a standard turbofan as there are electricity generation and conditioning losses. Also, the energy source is solely hydrocarbon fuel. A parallel hybrid electric architecture is mechanically complex due to the coupling of the electric motor and turbine engine. The series architecture is a strong contender because it is the most efficient with no added complexities while providing several of the benefits of a fully electric system. However, the challenge is to design a controller for matching or coupling the response time of motor and turbine.

The Parallel Power Split (PPS) hybrid-electric architecture is simple and relatively straightforward to implement. The hybridization factor for this architecture at sea level is expressed as

$$HF = \frac{Engine\ Shaft\ Power}{(Engine\ Shaft\ Power + Motor\ \ Shaft\ Power)} \qquad \textbf{Eq. 1}$$

The efficiency of the architecture is a function of the number of fuel and electric propulsion systems along with the hybridization factor. The efficiency also depends on the altitude because engine power output is altitude dependent. The efficiency of the PPS architecture with 2 motors and 2 engines, with a hybridization factor of 0.5, is about 55%. In general, the efficiency associated with this architecture is given by

$$\eta = [(1 - HF) * 0.39 + HF * 0.71] * 100\% \qquad \textbf{Eq. 2}$$

With higher efficiency and simplicity compared to other architectures, the PPS hybrid electric architecture shown in Figured 5(d) is selected in this effort.

1.3 Focus on Conceptual Design

This research is primarily focused on the conceptual design of a HEDiP regional transport aircraft (RTA) using a mature multidisciplinary design optimization (MDO) framework. The overall goal is to investigate potential benefits of HEDiP systems for optimal RTA designs.

A singular focus on conceptual design is derived from previous studies that show that more than two-thirds of the total Life Cycle Cost (LCC) is committed during the conceptual design phase. Figure 6 from Reference 13 depicts the cumulative percent of LCC against the product development phases. Note also that making design changes in the conceptual and preliminary design phases cost much less than in later phases. Note that meeting the stringent schedule and cost constraints of typical conceptual design efforts requires robust, quick, and accurate conceptual design tools.

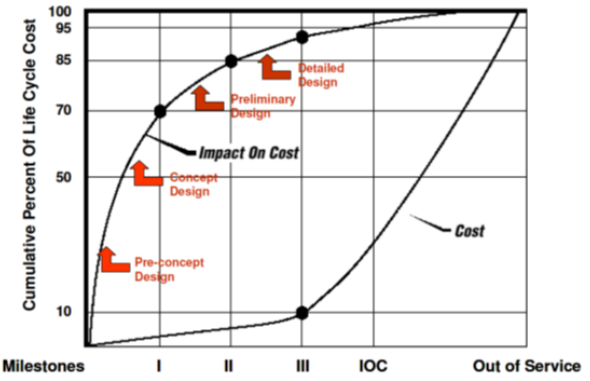

Figure 6. Dependence of cumulative Life Cycle Cost commits along with actual cost of product development phases. From Reference 13.

Multidisciplinary design and optimization (MDO) capabilities are relatively mature for conceptual design of traditional aircraft. However, further enhancements are needed for using them effectively to perform conceptual design of HEDiP aircraft. The present research has two specific objectives:

1. Enhance one of the mature MDO frameworks by incorporating a method for rapid and accurate estimation of multiple propeller effect on wing aerodynamics for HEDiP designs.
2. Use the enhanced framework to design a HEDiP RTA and quantify its potential benefits.

The overall methodology for achieving these objective is described in Section 2 followed by results and discussion in Section 3. A few concluding remarks in Section 4 complete the paper.

2.0 METHODOLOGY

2.1 Multidisciplinary Design Optimization Framework

Several MDO frameworks exist for aircraft conceptual design studies including NASA's OpenMDAO, NASA's Flight Optimization System (FLOPS), and Pacelab Aircraft Preliminary Design (APD). Although all these frameworks have been widely used for aircraft design, the Pacelab APD was selected for the present research. The selection criteria included capability, modularity, maturity, ease of update, Graphical User Interface (GUI), and reliability. Pacelab APD [14] is the product of a German company, PACE GmbH, now a part of TXT. For this research, PACE provided access to the state-of-the-art versions of the code, namely the Pacelab APD 6.2 and Pacelab APD 7 Alpha Release.

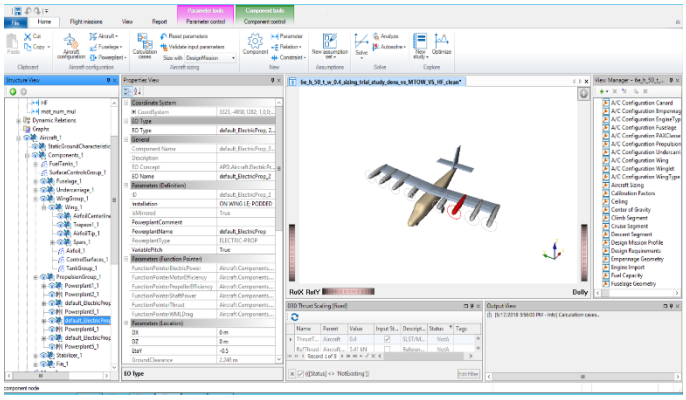

Figure 7. Pacelab APD 7 Alpha Graphical User Interface

Pacelab APD is widely utilized by researchers and innovators worldwide. It is continually updated to incorporate the most recent technological advances. An interesting feature is the unique solution engine that allows for a plethora of analysis and design possibilities. The approach is based on declarative design where the user decides the design methodology by prescribing the parameters that should be inputs and those that have to be estimated. Another interesting feature is the ability to rapidly setup design sensitivity studies, which is particularly useful in the design space exploration of radical aircraft designs.

APD offers a powerful GUI with a structured and easy to understand parameter prescription interface. Figure 7 depicts the user interface of Pacelab APD 7. The aerodynamics and weights modules are heavily inspired by the works of Torenbeek [15] and Raymer [16]. APD also leverages its extensive database to accurately estimate weights. APD includes a library of available computational methods which can be tapped for the analysis of the specified Engineering Object or aircraft component. Performance estimation of HEDiP aircraft require the implementation of modified methods. This is made easy with ready access to the computational library wherein individual methods can altered or simply replaced. Recent work by Cinar et al. [10] shows the potential of the Pacelab suite for incorporating hybrid electric systems into aircraft.

2.2 Wing Propeller Aerodynamics

The problem of wing mounted propellers has been extensively studied since the 1900s. Kroo [17] and Witkowski et al. [18] indicate that the mutual interaction of the flow between the wing and propeller could result in beneficial aerodynamic characteristics. Miranda and Brennan [19] share interesting insights on the propulsive benefits along with the induced drag reduction obtained from tip-mounted propellers and turbines. A more recent investigation by Veldhuis [20] further adds to the understanding of the aerodynamic interference between a propeller and a wing. Other works by Patterson [8] and Stoll et al. [4] also provide insights into analysis techniques and applications for wing-propeller interaction.

2.2.1 Wing Propeller Interaction Effects

The presence of a wing upstream of a pusher propeller has been understood to have positive contributions to the thrust produced by the pusher propeller. In comparison, the tractor propeller with the wing directly downstream of the propulsion system significantly alters the lift and induced drag characteristics. Studies by Miranda [19], Veldhuis [20], Epema [21], and Alba [22] have shown that the tractor propellers augment the aerodynamic efficiencies of the propeller–wing configurations, with increased lift and decreased induced drag.

The jump in dynamic pressure is primarily due to the axial component of the slipstream which increases the incoming freestream velocity; this results in increasing the forces on the wing. This is the primary component that is leveraged in the X-57 Maxwell DEP aircraft design. It is also interesting to note that the force increase is not just limited to the region of the wing directly behind the propeller, the effect also spreads across the span as shown in Figure 8 [20]. A possible explanation can be obtained by the potential flow theory. The augmented freestream velocity in the area subjected to the prop wash would mean that the wing vortex system would encounter a normal velocity of higher magnitude. This would naturally mean a greater circulation at these locations to satisfy the boundary conditions and thus more lift. As the axial component tends to act in the same direction on both halves of the propeller, i.e., the upward rotating blade and downward rotating blade regions, the sense of propeller rotation has no bearing on the change in wing aerodynamics due to the dynamic pressure increase. However, the performance change due to the axial component could be sensitive to the spanwise location of the propeller.

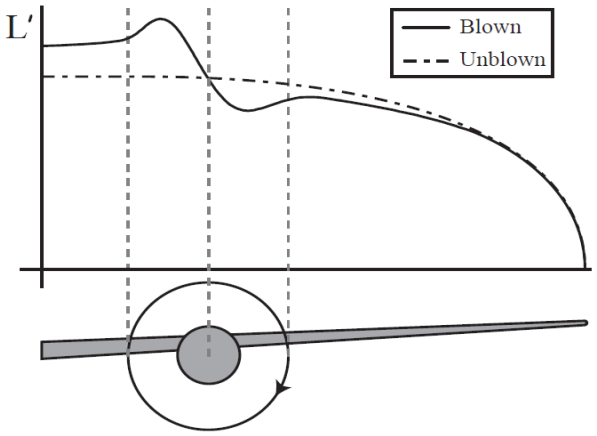

Figure 8. Variation in lift distribution due to the presence of a tractor propeller rotating in an inboard up manner. From Veldhuis [20].

The tangential component of the propeller slipstream acting in the circumferential direction (normal to the axial velocity) tends to modify the direction of the incoming freestream, and modifies the local sectional angle of attack. The direction of the swirl velocity follows the direction of motion of the propeller blade. An upward moving blade induces an upward velocity at the wing which increases the angle of attack at the sections of the wing behind the blade and thereby increases the local sectional lift. Similarly, the downward moving blade causes a local angle of attack to decrease and thereby reducing the lift produced there. This antisymmetric behavior observed in the lift distribution can also be observed for the induced drag, although in the opposing directions, with some exceptions. The upward going blade when modifying the freestream tilts the force vector forward, thereby creating a negative drag. The effect of the downwash from the downward going blade is to tilt the force vector backward, in case of positive lift and thus have a positive induced drag contribution. Veldhuis [20] argues that the forward tilted vector is strengthened while the backward tilted vector is weakened which leads to a net reduction in the induced drag in the presence of a propeller.

Although the wing immediately downstream of a propeller affects the propeller performance by modifying the upstream flow conditions, the current study considers only a “one-way interaction” model. That is, the effect of wing on the propeller is ignored, and only the effect of propeller slipstream on the wing is modeled by combining the effect of the jump in dynamic pressure and of the local sectional angle of attack as discussed in Section 2.3.

2.2.2 Wing Aerodynamic Estimation Techniques

Prediction of finite wing aerodynamic properties dates back to the early 20th century, initially established by Ludwig Prandtl [23] as an extension of the infinite wing results to a finite wing. Since then several techniques have evolved for estimating the aerodynamic performance of wings. The techniques offer varying levels of prediction accuracy and associated costs.

Wind tunnel testing is typically considered to be the most desirable for accurate estimation of wing aerodynamic characteristics. The expense in terms of resources and time, make it unsuitable for conceptual design trade studies and for applications based on optimization techniques. In contrast, computational methods can be fast and also well suited for optimization studies. Computational aerodynamics approaches have become increasing indispensable in modern day aircraft design and analysis. The increasing ease of

availability and affordability along with rapidly developing computational capability has only further strengthened such dependence. Computational Fluid Dynamics (CFD) methods based on the Navier-Stokes and Euler equations, provide high fidelity. However, the high computational costs and slow turnaround time of CFD restrict its effectiveness in early design exploration studies, and rapid and inexpensive methods are highly desirable.

Prandtl's Lifting Line Theory (LLT) is a very simple, easy to use, and inexpensive approach. Since its underlying assumption is potential flow, it cannot account for viscous effects; only lift and induced drag can be estimated. The LLT is most accurate for straight finite wings with high aspect ratios and incompressible flow regimes. The limitations of LLT are overcome by the Vortex lattice methods (VLM). As shown in Figure 9, the wing is represented by a mesh of horseshoe vortices. Circulation of each vortex is determined by imposing the no-normal-flow boundary condition at a control point on each panel. VLM solutions can be used to estimate lift, induced drag and moment coefficients of a wide variety of lifting surfaces with taper, sweep, dihedral and twist.

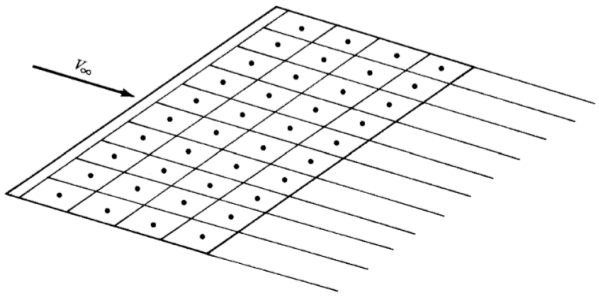

Figure 9. The system of horseshoe vortices representing a finite lifting surface, for VLM. From Anderson [24].

The VLMs are now widely used to estimate forces and moments of arbitrarily shaped wings with taper, sweep, dihedral and twist. Airfoil camber effects can also be accounted for. The VLMs offer the right trade-off between accuracy, speed, and capability for use in design exploration in the early stages.

2.2.3 Vortex Lattice Method Selection

A plethora of VLM codes has been developed for aircraft aerodynamic analysis, most of which have been validated for many configurations. For this study, several VLM codes were considered including Athena Vortex Lattice (AVL) [25], Tornado VLM [26], VSPAero [27], XFLR5 [28] and QuadAir [29].

Table 1
Decision Matrix for VLM code Selection

Attributes	AVL	QuadAir	VSPAero
Programming Language	FORTRAN	MATLAB	C++
Rotor/ Disk integration	No	No	Yes
Physics Conformity	Widely Demonstrated	Limited Demonstration	Widely Used
Execution Speed (1 Run)	Very Fast	Moderate	Fast
Learning Curve	Steep	Moderate	Above Moderate
Versatility/ Features	Good	Poor	Very Good
Ease of Adding New Features	Moderate	Easy	Hard
Ease of VnV/ Debugging	Moderate – Hard	Moderate	Very Hard
Community Trust	High	Low – Moderate	Moderate – High
Licensing	GNU GPL	N/A	NOSA

The decision matrix for the selection of a VLM code is shown in Table 1. VSPAero was a clear choice mainly because it could analyze wing-propeller configurations. In addition, it has a built-in mechanism to interface with external applications. The AVL, Tornado VLM and XFLR5 packages, while being very capable, are attached with a GNU General Public License [30], an interpretation of which proved to be unacceptable for Pacelab to integrate the code into their commercial APD software.

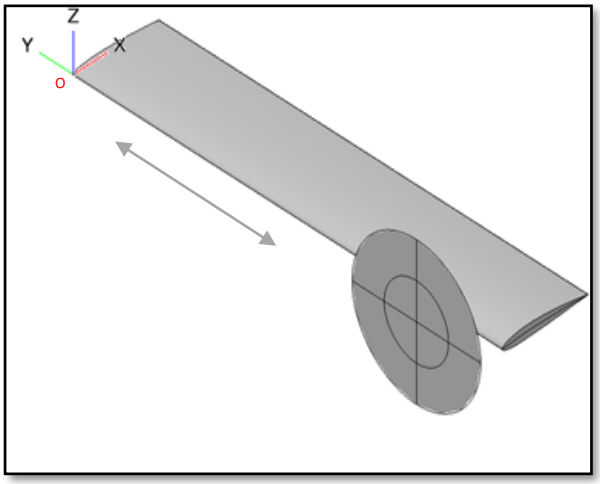

Figure 10. Propeller - Wing model used for spanwise variation study in VSPAero, the arrow indicates the direction of the propeller location variation

Table 2

Geometric parameters of the VSPAero Propeller - Wing model

Parameter	Value
Wing Chord (C)	2 m
Wing Semi-Span (b)	10 m
Airfoil	NACA0012
Propeller Diameter (Φ_P)	3 m
Advance Ratio (J)	0.8
Thrust Coefficient (T_C)	0.4
Propeller Vertical Location (Z - Axis)	0 m
Propeller Streamwise Location (X - Axis)	-0.5 m
Propeller Spanwise Location (Y -Axis)	-1 m to -10 m

A simple characterization of VSPAero was conducted for its propeller-wing aerodynamic prediction capabilities. A typical propeller-wing configuration shown in Figure 10 was considered,. Key parameters of the geometry are documented in Table 2. The results obtained from this study are depicted in the Figure 11, where the lift and drag coefficients are plotted against the propeller location along the semi wing span. The results in the figure clearly show erratic trends. The method, therefore, is not suitable for any kind of optimization study. Also, noticeable sensitivity to the predicted results is observed when the propeller location is varied even by 1% of the wing span at certain locations. The exhibited characteristics are well beyond the expected behavior for such a variation, and it was concluded that VSPAero was less than satisfactory for use in the current investigation.

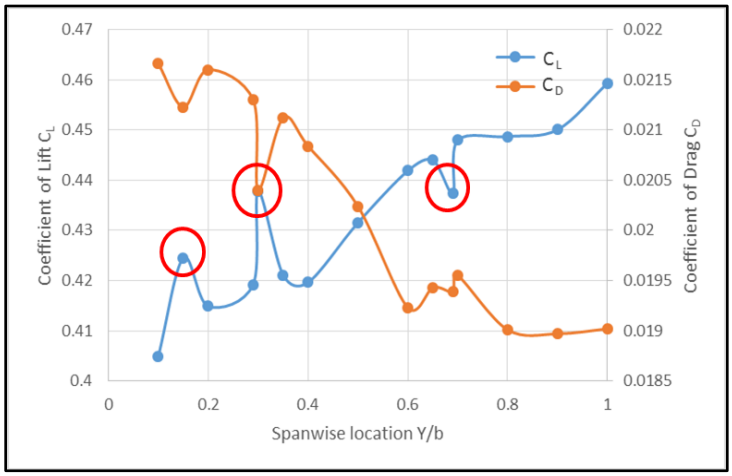

Figure 11. Computed lift and drag coefficients for various spanwise loctions of the propeller using VSPAero that exhibit an unacceptable erratic trend.

To meet the need of a robust aerodynamic estimation software, the development of Wing Aerodynamic Simulation with Propeller Effects (WASPE) code was undertaken. For this development, QuadAir, developed by Roberto A. Bunge at Stanford University, was selected, which utilizes the MATLAB platform. QuadAir, while lacking the capability to account for propeller slipstream, rated well for the implementation of new methods and modifications as shown in Table 1.

2.2.4 Propeller Slipstream Modeling

The quest for a robust and quick propeller slipstream development tool that could be effectively employed in conceptual design and optimization studies led to the consideration of the widely used software XROTOR. It is a propeller analysis and design tool developed by Drela [31]. XROTOR provides circumferentially-averaged time-independent results to the unsteady propeller problem. Axisymmetric distribution of the axial and swirl induced velocities at a required refinement of radial stations can be obtained for low computational expenses. Therefore it was considered an effective method for propeller induced velocity estimation for this research.

The XROTOR code also accounts for the effects of the geometric characteristics of the propeller being modelled including the number of blades, twist angles and chord distributions from the root to tip, while accounting for the presence of a propeller hub where induced velocities are modelled as non-existent. Its potential formulation is an extension of the Goldstein solution to an arbitrary number of blades, and arbitrary radial load distributions is used for the computation of the required velocities with required radial refinement. Individual blades are modelled as lifting lines, with bound vortices placed radially along the span, along with helically developing trailing vortices being extended from each blade, thereby solving for a rigid wake of helicoidal nature. XROTOR can also be used to simulate co-rotating and contra-rotating propellers. Such a capability would be highly desirable for some design studies.

The slipstream velocities are modelled in a cylindrical propeller streamtube, thereby neglecting the contraction and shape of the developing slipstream. While XROTOR has several desirable features, it also has some key shortfalls such as the absence of viscous effects and the lack of compressibility effects.

2.3 Wing Aerodynamic Simulation with Propeller Effects (WASPE)

WASPE is a modified version of QuadAir, a VLM code, which integrates propeller slipstream data into the analysis. The slipstream data may be from (i) a software such as XROTOR; (ii) user supplied experimental data; or (iii) analytical data. WASPE, along with facilitating the propeller effects, significantly modifies the QuadAir code by altering data flow and methods for estimating forces, moments and circulation. Compressibility corrections, spanwise distribution of the aerodynamic coefficients and estimation of the stability derivatives for asymmetric configurations are also enabled. Data transfer thorough file exchange for user ease along with effective communication with external modules is introduced.

WASPE requires a few modifications from the traditional VLM formulation to represent lifting surfaces subjected to the slipstream of the tractor propeller(s). The propeller–wing interaction effects can be simulated by changing the boundary conditions. Here the velocity at panel control points is altered by adding the induced velocities generated by the upstream propeller(s). This velocity is given as

$$V = V_{induced} + V_{\infty} + V_{propeller} \qquad \textbf{Eq. 3}$$

Propellers are modelled in WASPE by transforming the radial slipstream data in the propeller reference plane into Cartesian velocity components in the WASPE plane of reference. WASPE identifies the control points affected by the slipstream of a propeller and determines the velocity change at these points through a linear interpolation of the propeller slipstream data, and is repeated for all the propellers. The change in velocity components is given by

$$V_x = u_{induced} + u_{\infty} + V_{axial} \qquad \textbf{Eq. 4}$$

$$V_z = w_{induced} + w_{\infty} + V_{tangential} \qquad \textbf{Eq. 5}$$

This change in velocity is reflected in the change in circulation in order to satisfy the Neumann boundary conditions. Equation 6 gives the panel circulations as

$$\Gamma = [AIC]^{-1}(-V_{\infty}.n - V_{propeller}.n) \quad \textbf{Eq. 6}$$

The lift and induced drag forces now become

$$l = \rho\Gamma(V_{axial} + u_{\infty} + u_{induced}) \quad \textbf{Eq. 7}$$

$$d_{ind} = \rho\Gamma(V_{tangential} + w_{induced}) \quad \textbf{Eq. 8}$$

Note that the change in these forces affects the moments as well.

2.3.1 Slipstream Data Parsing

A typical axial velocity profile of the slipstream is shown in Figure 12. This input set is associated with a certain radial refinement depending on the source of the slipstream, i.e., the number of discrete radial locations where induced velocity information is available. The input is converted into another data set with the same refinement used by the lifting surfaces of WASPE.

The panel locations are identified by tracking the first spanwise panel, the control point of which is under the influence of the propeller slipstream. This is determined by the following equation

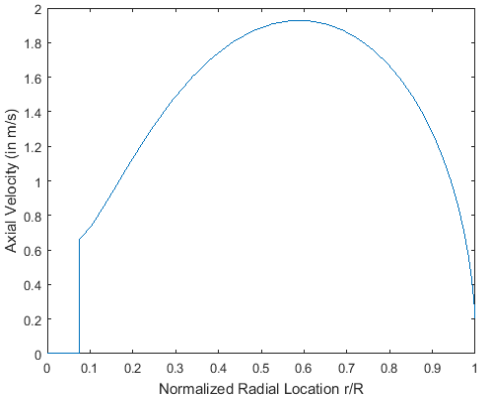

Figure 12. Sample input axial velocity profile

$$R_1 = Round\left(\frac{P_y - real\left(\sqrt{r_p^2 - P_z^2}\right)}{\Delta b}\right) \quad \textbf{Eq. 9}$$

The values $P_y\ and\ P_z$ are the spanwise and vertical locations of the propeller, r_p is the radius of the propeller and Δb is the width of the equally spaced panels. Similarly, the last panel to experience the slipstream is identified by

$$R_2 = Round\left(\frac{P_y + real\left(\sqrt{r_p^2 - P_z^2}\right)}{\Delta b}\right) \quad \textbf{Eq. 10}$$

If either of the panel locations is estimated to occur outside the lifting surface limits, such as the case of wingtip mounted propellers, the panel location(s) violating this limit are reset to the panel closest to the limit, such as the wingtip panel.

The panels subjected to the slipstream are identified as every spanwise and chordwise panel between the identified first and last panels $R_1 and\ R_2$ as shown in Figure 13. The

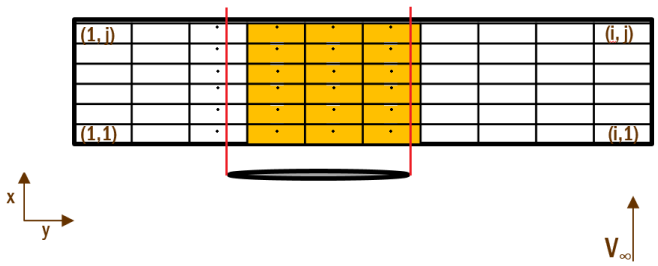

Figure 13. Schematic for identifying panels subjected to prop wash. Yellow panels are affected by propeller, others are not.

respective control point locations are projected on to the propeller plane, the velocities experienced on them are then determined using a simple linear interpolation scheme.

The normalized radial location in the propeller reference plane P_L of the control points are given by Equation 11 where R_l is the calibrated panel location which is set to 0 at the center of the propeller disk.

$$P_L = \sqrt{P_z^2 + \left(\sqrt{r_p^2 - P_z^2} - (R_l * \Delta b)\right)^2} \qquad \textbf{Eq. 11}$$

Figure 14 shows the additional slipstream velocity as seen by WASPE, where the slipstream with 30 data points is represented by two 5-point curves. In order to ensure that all features of the slipstream are accurately captured, panels on the lifting surface must be densely packed. The required density must be determined on a case by case basis as a tradeoff between computational speed and accuracy. Implementation of an unequal spacing scheme could thus prove to be a very useful future addition to WASPE.

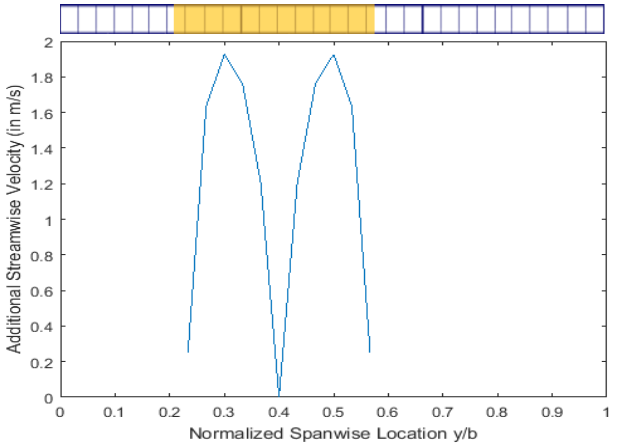

Figure 14 Additional streamwise (X) Velocity as seen by WASPE control points.

2.4 WASPE Coupling with Pacelab APD

The flow of data in the coupling of WASPE with Pacelab APD is shown in Figure 15. The procedure allows the use of aerodynamic data from one of two sources: (a) a dynamic query for updated data set from WASPE for each iteration, and (b) a Reference Drag Polar (RDP) generated with WASPE for the initial estimate. The choice of data source is designated as a user input. The tradeoff between the two sources is accuracy and speed, with each drag polar containing

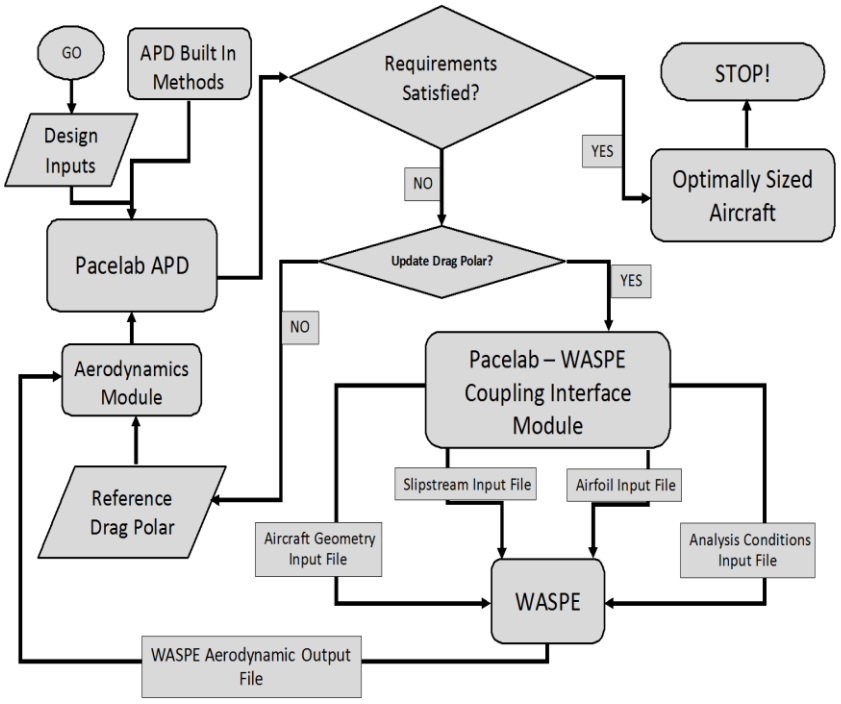

Figure 15. Flowchart depicting WASPE-APD coupling

about 50 data points as altitude, speed and angle of attack are varied. The use of a single RDP generated with an initial estimate of the wing geometry would be several times faster, depending on the number of iterations, than a dynamic query for the updated drag polar from WASPE.

The methodology for this study is to obtain a converged solution using the reference drag polar where the geometry is allowed to vary. This is followed by further refinement of the performance characteristics using updated data from WASPE with the converged solution as the analysis case, thereby striking balance between speed and accuracy. This process could be repeated multiple times if required for a higher degree of accuracy.

3.0 RESULTS AND DISCUSSION

3.1 WASPE Validation

WASPE has been validated by comparing its predictions to experimental data of Veldhuis [20]. Figure 16 shows the geometry utilized for this comparison. Further details of the geometry can be seen in Reference 20. A single propeller–wing configuration is considered; the direction of propeller rotation is inboard up. The spanwise distribution of the sectional lift coefficient is depicted in Figure 17. The computed and measured data compare well. The predicted behavior is in accordance with the theory of propeller–wing interaction which suggests that the upward rotating blade increases local lift while the downward moving blade reduces it. Note that there is no experimental data to compare the sectional induced drag distribution.

In Figure 18, the computed variation of the wing lift coefficient with angle of attack is compared with measured data. The variation of the computed induced drag coefficient with lift is shown in Figure 19, and it exhibits the expected behavior.

Lack of experimental data for multiple propeller wing aerodynamics restricted the validation to a single wing propeller case.

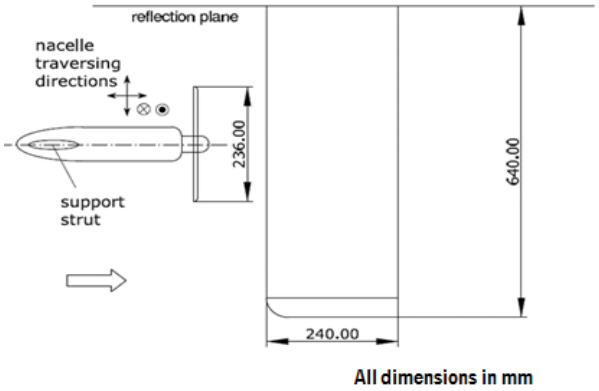

Figure 16. The geometry used for WASPE validation. From Veldhuis [20]

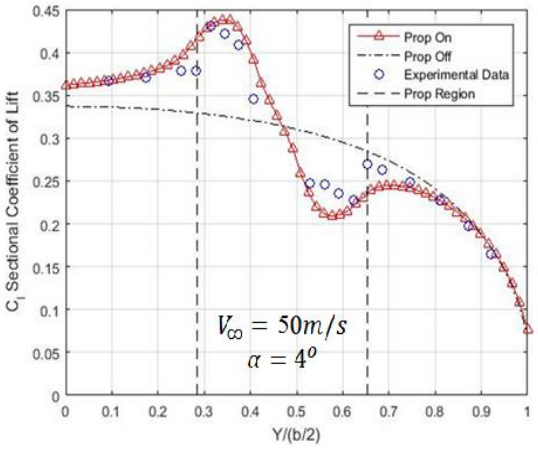

Figure 17. Comparison WASPE sectional lift coefficient to experimental data. Experimental data from Veldhuis [20].

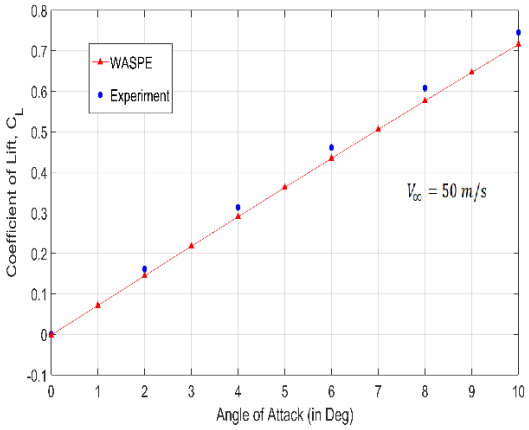

Figure 18. Comparison of WASPE and experimental wing lift coefficient. Experimental data from Veldhuis [20].

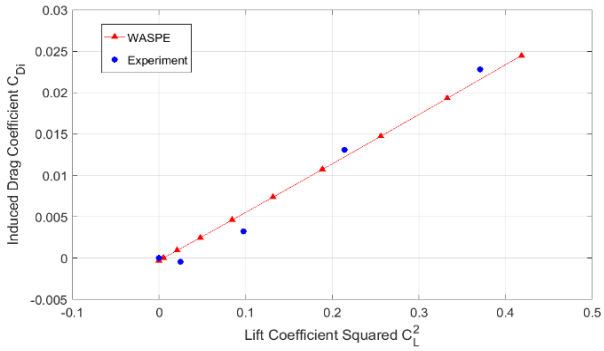

Figure 19. Comparison of WASPE and wing induced drag coefficient. Experimental data from Veldhuis [20].

3.1.1 WASPE Current Capabilities and Limitations

The current capabilities of WASPE include:

- Estimation of the effect of multiple propellers on wing aerodynamics
  - Symmetric and asymmetric configurations and/or flight conditions
  - Wing lift, drag, pitching moment and rolling moment coefficients and distribution across the span
  - Effect of spanwise locations of propellers on wing aerodynamic data
- Kutta–Joukowski and Trefftz plane estimates of drag
- Compressibility Corrections
  - Prandtl–Glauert
  - Laitone
  - Karman–Tsien

The current limitations of WASPE are

- No shocks or viscous effects
- Current version cannot model the effect of vertical and streamwise propeller locations
- Effect of wing on propellers is not modeled

On balance, WASPE is considered adequate for HEDiP aircraft conceptual design studies.

3.2 Hybrid Electric Regional Multi-Propeller Integrated Transport (HERMiT) Aircraft

In this section, the design of a Hermit aircraft is described, and benefits associated with the use of HEDiP technologies are identified. Results are presented to illustrate the sensitivity of the design to battery storage and energy source distribution parameters. Also, benefits of the wing-propeller interaction arising from distributed propulsion are investigated.

3.2.1 Baseline Aircraft: Specifications and Mission

The de Havilland Canada DHC-6-400 Twin Otter aircraft is used as the baseline regional aircraft. It is a twin turboprop conventional regional transport aircraft powered by Pratt & Whitney single stage free-turbine propulsion systems coupled with three bladed reversible pitch Hartzell propellers. The propulsors are mounted on a high wing. The Twin Otter consists of a metal airframe and a tricycle landing gear. The design specifications are summarized in Table 3.

The HERMiT aircraft design mission is the same as that of the Twin Otter. The Twin Otter has a maximum range of 400 NM with a maximum of 19 passengers. Demonstration of the capabilities of the HEDiP RTA for the same mission would help quantify the potential benefits. Figure 20 shows the primary mission profile and Table 4 contains some of the key parameters for specifying the mission.

Table 3
Baseline Twin Otter Specifications

Mission Payload	19 PAX + 2 crew (1,474 kg)
MTOW	5,670 kg
OEW	3,377 kg
MLW	5,579 kg
Span	19.8 m
Area	41.98 m^2
Wing Loading	135 kg/m^2
Wing Airfoil Section	NACA 63A516 Mod
Thrust-to-Weight Ratio	0.54
Max Range with Mission Payload	400 NM
Ceiling	8138.16 m (26,700 ft.)
Cruise Altitude	3048 m (10,000 ft.)
Max. Cruise Speed	182 KT
Propulsion	2x PT6A-34, 650 SHP
Max. Fuel	1431 L

The same mission was recreated in Pacelab APD 6.2 in order to validate the predictions of this MDO framework. It was determined that the Twin Otter model performance and parameters were in close agreement with the original aircraft specifications. Note also that HERMiT would be designed to accommodate a fuel reserve to enable a 45-minute hold at cruise level, for a fair comparison with the Twin Otter.

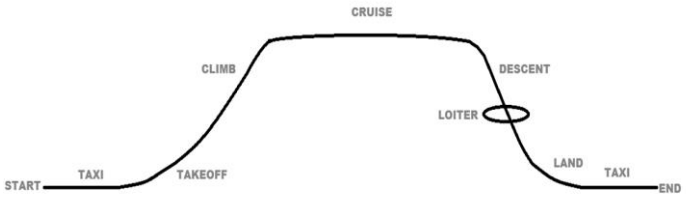

Figure 20. HERMiT RTA design mission. Range considered from start to end.

Table 4
Key Mission Parameters for HERMiT

Mission Range	400 NM
HERMiT Payload	19 PAX + 2 Crew (1474 kg)
HERMiT Cruise Altitude	3048 m (10,000 ft.)
Cruise Speed	182 KT (93.6 m/s)
Max Payload (For Payload - Range)	1900 kg
Reserve Mission	45 min Loiter at Cruise

3.2.2 HERMiT 2E

HERMiT 2E is a hybridized variant of the baseline Twin Otter with 4 powerplants: 2 electric motors and two engines. The target of the design is to match the specified range and payload of the Twin Otter. The wing geometry is not unchanged for this design. Also, the benefits of propeller-wing interaction were not accounted for. This case assesses the practicality of developing an aircraft using hybrid electric propulsion without any other benefits for an EIS using technologies in the 2025 timeframe. In the 3-view of this design shown in Figure 21, the inboard powerplants in red depict the turboprop engines and the outboard podded powerplants are electric motors.

Sensitivity studies on HERMiT 2E were carried out using Pacelab APD. The objective was to investigate changes in the maximum take-off weight (MTOW) due to changes in two design variables, hybridization factor and battery specific energy. The variation of MTOW with battery energy density is shown in Figure 22 for a HF of 50%. The trend reveals that in the 2025 timeframe, with a battery energy density of about 0.31 kWh/kg, HERMiT 2E has more than twice the MTOW of the baseline, making an EIS with 50% hybridization factor impractical. Wheras HERMiT 2E is not practical for 2025, the carpet plot in Figure 23 shows that it still offers better performance than more electric (higher HF) variants. As evident from the trends observed in the carpet plot, more electric would mean a greater weight penalty.

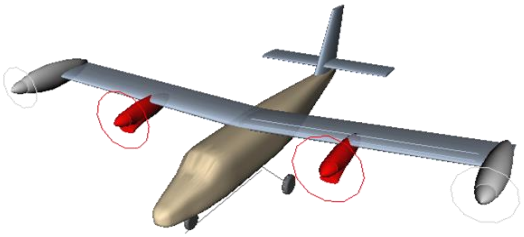

Figure 21. A 3-view of HERMiT 2E

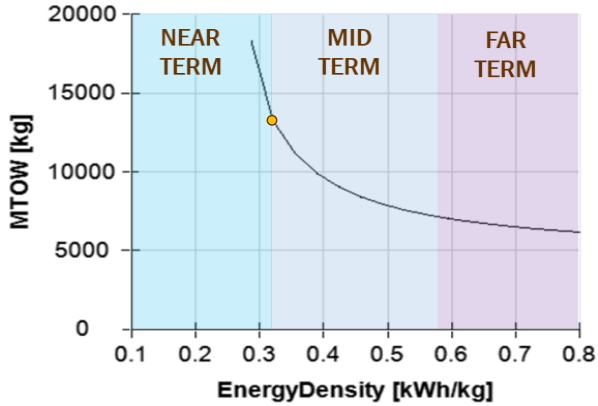

Figure 22. HERMiT 2E Sensitivity to battery energy density at HF = 0.5.

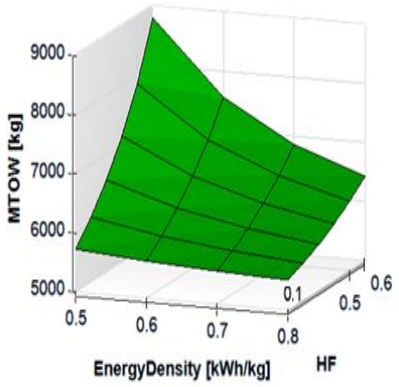

Figure 23. HERMiT 2E MTOW sensitivity to hybridization and battery technology advancements.

This investigation also revealed that, as one might expect, a design with lower hybridization factor would be less dependent on energy density. Similarly, higher levels of hybridization show higher dependence on battery energy density.

3.2.3 HERMiT 6E/I

Encouraged by the results of the HERMiT 2E investigation, a series of HERMiT 6E aircraft were designed next that leverage eight propulsion systems of which six are electric motors. The variant that exploits the benefits of distributed propulsion in addition to hybrid electric system is designated as HERMiT 6E/I. The HERMiT 6E/I is designed with a target Entry-Into-Service (EIS) timeframe of 2030, utilizing technologies with TRL of 6 or higher by 2025.

For the initial step, a reference drag polar generated from WASPE for the HERMiT 6E wing-propeller configuration is used. The resulting design is refined by using the drag polar from WASPE being run dynamically with APD. This approach reduces the number of WASPE calculation cases and thereby saving considerable computing time. A typical WASPE batch run when coupled with APD requires around 75 calculation cases for each iteration.

The aircraft design mission remains the same as that for the Twin Otter described in section 3.2.1. The hybridization factor for the 6E/I variant is 0.3. The wing span is fixed to the HERMiT 6E value, also the mean aerodynamic chord was varied. The key design parameters of the HERMiT 6E/I are compared with that of the baseline Twin Otter in Table 5.

The result of leveraging the benefits of distributed propulsion along with the PPS hybrid electric propulsion system is a 29% reduction in the wing area when compared to the baseline Twin Otter. Also, the energy cost associated with the operation of the aircraft per trip is substantially reduced. The improvements in HERMiT 6E/I come at the slight penalty of MTOW for the same design mission.

Table 5
Comparison of Twin Otter and HERMiT 6E/I Design

	DHC–6–400	HERMiT–6E
MTOW	5670 kg	6175 kg
Energy Cost	$1935	$1045
Payload	19 PAX + 2 crew	19 PAX + 2 crew
Range	400 NM	400 NM
Altitude	10,000 ft.	10,000 ft.
S_{ref}	41.98 m^2	29.7 m^2
Fuel	1466 L	560 L
Energy Density	-	0.31 kWh/kg
Electric Energy	-	450 kWh
Timeline	In Service	EIS 2030

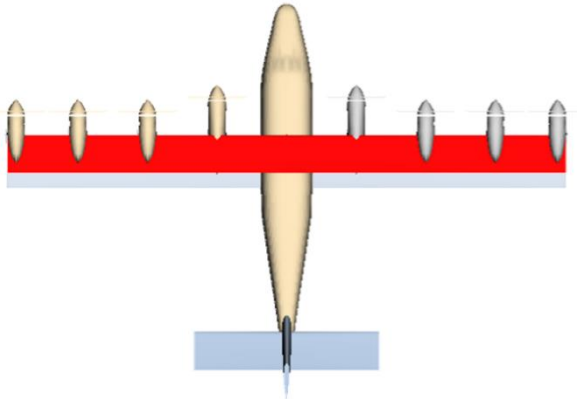

Figure 24. Comparison of baseline Twin Otter and HERMiT 6E/I, the reduced 6E/I wing area is depicted in red.

Figure 24 shows the HERMiT 6E/I superimposed over the baseline Twin Otter. It illustrates the reduction in wing area; the smaller wing of the 6E/I aircraft is highlighted in red. The significantly reduced wing area is the directly related to the improved aerodynamic efficiency of the wing due to the effect of the eight propeller slipstreams. Reduced wing area means a lower thrust-to-weight ratio along with a 45% reduction in required power.

4.0 CONCLUDING REMARKS

The overall goal of the present study was to investigate potential benefits of optimal regional transport aircraft based on HEDiP systems. The primary focus was on the conceptual design of a HEDiP RTA using a mature MDO framework so that needed enhancements could be easily made to accommodate the specific needs of integrating HEDiP systems.

The Pacelab APD MDO framework was selected, and its aerodynamics module was modified to account for the effect of multiple propellers on wing aerodynamics. This required the development of the Wing Aerodynamic Simulation with Propeller Effects (WASPE) code, and coupling it with the APD. The WASPE code was developed by modifying a state-of-the-art VLM code, QuadAir, by incorporating the effect of multiple propeller slipstreams on the wing. This was accomplished by adding the propeller induced velocities to update the total velocities at the control points on the vortex lattice panels directly behind the propellers. WASPE was validated using the available experimental data, and the code was successfully coupled with the Pacelab APD.

The Pacelab APD, coupled with WASPE, was first used to develop the HERMiT 2E series of RTA. This effort demonstrated the anticipated benefits of HEDiP technologies over conventional aircraft, and provided a better understanding of the sensitivity of RTA designs to battery technology and level of hybridization. The conceptual design of HERMiT 6E/I was then conducted to quantify the benefits of HEDiP systems over an existing baseline Twin Otter aircraft. The results showed that a comparable performance could be obtained with more than 50% saving in trip energy costs for a small MTOW penalty. The fuel burn was also significantly reduced, with HERMiT 6E/I requiring only about 38% of the mission fuel borne by the baseline. This means a correspondingly lower direct atmospheric heat release, reduction in carbon dioxide and NO_x emissions along with reduced energy consumptions, all of which are the key subsonic technology improvement goals in the NASA Strategic Implementation Plan 2017.

Implementation of HEDiP technologies in future RTAs indeed brings some very attractive improvements both from economic and environmental standpoints. The demonstration of the feasibility and economic practicality of HERMiT 6E/I for an entry-in-service date of 2030 suggests that HEDiP technologies can be utilized in not too distant future to reap many benefits of the all-electric aircraft without having to wait until much later when battery energy density reaches a high enough level for an all-electric RTA to be practical.

ACKNOWLEDGMENTS

This research was partially supported by a grant from the Virginia Tech Institute for Critical Technology and Applied Science (ICTAS) to the Kevin T. Crofton Department of Aerospace and Ocean Engineering with Prof. Rakesh Kapania as the Principal Investigator. We wish to acknowledge Prof. Kapania's support and encouragement of this work. We also acknowledge the generous support of Mr. Alexander Schneegans, President, Pace America Inc. The authors would like to thank Dr. Darcy Allison of the Air Force Research Laboratory for his time, thoughtful critiques, and constructive suggestions. The views and conclusions contained herein are those of the authors.

REFERENCES

1. *"NASA ARMD Strategic Implementation Plan 2017 Update"*, 2017.
2. *"Electric Propulsion Aircraft"*, NASA Armstrong, June 2016, https://www.nasa.gov/centers/armstrong/multimedia/imagegallery/electric_propulsion_aircraft/index.html, Accessed: September 2016.
3. Borer, N.K., Moore, M.D., and Turnbull, A., *"Tradespace Exploration of Distributed Propulsors for Advanced On-Demand Mobility Concepts"*, 14th AIAA Aviation Technology, Integration, and Operations Conference, American Institute of Aeronautics and Astronautics, Atlanta, Georgia, 16–20 June 2014. AIAA 2014-2850
4. Stoll, A.M., Bevirt, J., Moore, M.D., Fredericks, W.J., and Borer, N.K., "*Drag Reduction through Distributed Electric Propulsion"*, Aviation Technology, Integration, and Operations Conference, American Institute of Aeronautics and Astronautics, Atlanta, Georgia, July 2014. AIAA 2014-2851
5. Hepperle, M., "*Electric Flight – Potential and Limitations",* DLR, Institute of Aerodynamics and Flow Technology, Lisbon, October 2012.
6. Moore, M.D. and Fredericks, W.J., "*Misconceptions of Electric Aircraft and their Emerging Aviation Markets"*, 52nd Aerospace Sciences Meeting, AIAA SciTech Forum, American Institute of Aeronautics and Astronautics, National Harbor, Maryland, January 2014. AIAA 2014-0535
7. Gohardani, A.S., "*A synergistic glance at the prospects of distributed propulsion technology and the electric aircraft concept for future unmanned air vehicles and commercial/military aviation",* Progress in Aerospace Sciences, Vol. 57**,** 2013. pp. 25-70.
8. Patterson, M.D., "*Conceptual Design of High-Lift Propeller Systems for Small Electric Aircraft"*, Ph.D. Thesis, School of Aerospace Engineering, Georgia Institute of Technology, August 2016.
9. Del Rosario, R., *"A Future with Hybrid Electric Propulsion Systems: A NASA Perspective,"* Turbine Engine Technology Symposium, Strategic Visions Workshop, Dayton, OH, September 11, 2014.
10. Cinar, G., Mavris, D.N., Emeneth, M., Schneegans, A., and Fefermann, Y., *"Development of Parametric Power Generation and Distribution Subsystem Models at Conceptual Aircraft Design Stage"*, 55th AIAA Aerospace Sciences Meeting, AIAA SciTech Forum, American Institute of Aeronautics and Astronautics, Grapevine, Texas, 9 - 13 January 2017. AIAA 2017-1182

11. Strack, M., Zill, T., and Nagel, B., *"Integration of Hybrid Propulsion System In A CS23 Commuter Design"*, 30th Congress of the International Council of the Aeronautical Sciences, Daejeon, Korea, September 25-30, 2016.
12. Ganesh, R. V., *"Design Optimization of a Regional Transport Aircraft with Hybrid Electric Distributed Propulsion Systems",* Master's Thesis, Kevin T. Crofton Department of Aerospace and Ocean Engineering, Virginia Polytechnic Institute and State University, May 2018.
13. Raj, P. and Friedman, A.M., "*On timely and cost-effective prediction of aerodynamic data to meet aircraft design needs*", RAeS Applied Aerodynamic Conference, Royal Aeronautical Society, Bristol, United Kingdom, 22-24 July 2014.
14. *"PACELAB APD 6.2 User Documentation"*, PACE GmbH, 2017.
15. Torenbeek, E., *"Synthesis of Subsonic Airplane Design"*, Delft University Press, 1984. ISBN: 9024727243
16. Raymer, D., *"Aircraft Design: A Conceptual Approach"*, 5th Edition, American Institute of Aeronautics and Astronautics, 2012, Reston, Virginia. ISBN: 1600869114
17. Kroo, I., "*Propeller Wing Integration for Minimum Induced Loss",* Journal of Aircraft, Vol. 23**,** No. (7), July 1986. pp. 561-565.
18. Witkowski, D.P., Lee, A.K.H., and Sullivan, J.P., "*Aerodynamic interaction between propellers and wings",* Journal of Aircraft, Vol. 26**,** No. (9), September 1989. pp. 829-836.
19. Miranda, L.R. and Brennan, J.E., "*Aerodynamic Effects of Wing Tip Mounted Propellers and Turbines"*, 4th Applied Aerodynamics Conference, American Institute of Aeronautics and Astronautics, San Diego, California, June 9–11 1986. AIAA 86-1802
20. Veldhuis, L.L.M., "*Propeller Wing Aerodynamic Interference"*, Ph.D. Thesis, Department of Aerospace, Delft University of Technology, June 2005.
21. Epema, H.K., "*Wing Optimisation for Tractor Propeller Configurations"*, Thesis, Faculty of Aerospace Engineering, Delft University of Technology, June 2017.
22. Alba, C., "*A Surrogate – Based Multi – Disciplinary Design Optimization Framework Exploiting Wing – Propeller Interaction"*, Master's Thesis, Faculty of Aerospace Engineering, Delft University of Technology, February 2017.
23. Prandtl, L., "*Essentials of Fluid Dynamics"*, Hafner Publishing Company, 1952.
24. Anderson Jr., J.D., "*Fundamentals of Aerodynamics"*, 5th Edition, McGraw –Hill Inc, 1991, Boston, Massachusetts. ISBN: 0073398101
25. Drela, M. and Youngren, H., *"Athena Vortex lattice (AVL)"*, http://web.mit.edu/drela/Public/web/avl/, Accessed: 25 February, 2017.
26. *"Tornado VLM"*, http://tornado.redhammer.se/, Accessed: 25 February 2017.
27. *"OpenVSP (VSPAero)"*, http://openvsp.org/, Accessed: 25 February, 2017.
28. *"XFLR5"*, http://www.xflr5.com/xflr5.htm, Accessed: 25 February, 2017.
29. Bunge, R.A., *"QuadAir"*, May 2014, https://github.com/rbunge/QuadAir, Accessed: 22 August 2017.
30. *"GNU General Public License"*, Free Software Foundation, June 2007, https://www.gnu.org/licenses/gpl-3.0.en.html, Accessed: November 2017.
31. Drela, M. and Youngren, H., *"XROTOR"*, http://web.mit.edu/drela/Public/web/xrotor/, Accessed: 23 January, 2017.